The Effect of the Loading Rate on the Full-Field Strain Distribution on Intervertebral Discs

The Effect of the Loading Rate on the Full-Field Strain Distribution on Intervertebral Discs

Maria Luisa Ruspi, Luca Cristofolini

PMID: 32601688 DOI: 10.1115/1.4047662

The effect of the loading rate on the full-field strain distribution on the surface on the intervertebral discs

Ruspi Maria Luisa[1], Cristofolini Luca[1]

[1] Department of Industrial Engineering, School of Engineering and Architecture, Alma Mater Studiorum – Università di Bologna, Bologna, Italy

Corresponding author:
Luca Cristofolini
Department of Industrial Engineering
University of Bologna
Via Umberto Terracini 24-28
40131 Bologna, Italy
e-mail: luca.cristofolini@unibo.it

ABSTRACT

Contrasting results are reported when the spine is tested at different strain rates. Tissue specimens from the ligaments or the intervertebral discs (IVD, including annulus fibrosus and nucleus pulposus) exhibit higher stiffness and lower dissipation at high strain rates. Counterintuitively, when spine segments are tested at high rates, the hysteresis area and loop width increase. It is unclear how the load is shared between the different structures at different loading rates. The hypotheses of this study were: (i) As the IVD stiffens at higher loading rates, the strain distribution around the disc would be different depending on the loading rate; (ii) Pre-conditioning attenuates the strain-rate dependency of the IVD, thus making differences in strain distribution smaller at the different rates.

Six segments of three vertebrae (L4-L6) were extracted from porcine spines and tested in presso-flexion at different loading rates (reaching full load in 0.67s, 6.7s and 67s). The full-field strain maps were measured using digital image correlation on the surface of the IVDs from lateral. The posterior-to-anterior trends of the strain were computed in detail for each IVD, and compared between loading rates.

The values and the direction of principal strain on the surface of the IVDs, vertebrae, and endplates remained unchanged at different rates. In the transition zone between IVD and vertebra, only slight differences due to the loading rate appeared but with no statistical significance. These findings will allow better understanding of the rate-dependent behaviour and failure of the IVD.

Keywords:

Intervertebral disc, Digital Image Correlation, Loading rate, Conditioning, Annulus fibrosus, Full-field strain distribution.

1. INTRODUCTION

The anulus fibrosus (AF) is the external part of the intervertebral disc (IVD) and consists of elastic collagen fibers, which wrap the nucleus pulposus (NP) and is attached to the endplates of the cranial and caudal vertebrae [1]. The NP consists of a gelatinous structure rich of poly-anionic proteoglycans situated in the central part of the IVD. The great water content of the NP contributes to dampen the spinal loads and working as a shock absorber when transferring the loads to the surrounding tissues. The load is transferred from the NP to the AF because the nucleus can be likened to a sealed hydraulic system, in which a small loss of fluid leads to a large drop in pressure. In order to map the pressures in the NP and within the AF of the human spinal discs, pressure transducers were used by Ranu *et al.* [2]. The pressure in the NP generates tensile stress in the surrounding AF [2]. Pressures in the NP and strains in the AF were linearly related to each other and to the applied loads. Strains of the vertebral body had a corresponding trend with the applied compressive loads, when the partial vertebral column was loaded up to the point of bony fracture. The kinematics of the IVD is complex: when the spine is flexed, the NP moves posteriorly, while when the spine is extended, the NP moves anteriorly [3, 4].

Soft tissues are known to be viscoelastic, exhibiting generally higher stiffness and lower dissipation at high strain rates [5]. The NP exhibits also different characteristics in response to shear deformations depending on the loading rate; consequently, the NP can be described either as a fluid or as a solid [6]. With the application of the same load, a higher loading rate causes a stiffening of the NP and therefore a smaller deformation of the IVD. Conversely, a lower rate causes a softening of the NP and a greater deformation of the IVD [7, 8]. *In vivo* studies, measuring the intradiscal pressure with a pressure transducer, showed that an increase of the loading rate causes a higher hydrostatic

pressure and lower solid matrix strains [9, 10]. Also the tissue of the AF exhibits strong viscoelasticity: there is a significant increase in the modulus at linear region at higher strain rates [9, 11, 12]. However, in destructive tests, no significant differences in ultimate stress, ultimate strain and strain energy density were observed at different strain rates [11]. The rate dependency in mechanical properties of the AF could be primarily due to collagen fibers and not to the annulus matrix component [11].

When a multi-vertebra spine segment or a functional spinal unit (FSU) is tested, the structural behaviour (stiffness, range of motion) can be expected to depend on the loading rate [7, 13-17]. High rates involve an increase of stiffness of the structures of the spine due to the viscoelastic response of the different tissues [9]. The ability of the IVD to dissipate energy increases at lower strain rates [7]. Regarding the range of motion and the neutral zone, no differences were found by Wilke *et al.* using different rotational rates (0.6°-5.1°/second) [17]. Race *et al.* [7] examined the hysteresis of the load-displacement graphs indicating the energy dissipation of the IVD.

Since parameters related to stiffness are likely to be affected by loading rate, a study [18] examined the effect of those factors on motion parameters derived from continuous motion data. When the loading rate increased there were significant increases in hysteresis area, in hysteresis loop width, and in the upper and lower transition zone slopes [18]. At the same time transition zone width decreases significantly. These effects on the hysteresis and on the transition zone are quite counter intuitive since they seem to contradict the consolidated findings at the tissue level, and past observations about the structural stiffness of the IVD as a whole.

While the structural behaviour of spine segments and the tissue-level viscoelastic properties have been extensively investigated, little is known at an intermediate scale. To investigate the strains on the AF surface and the disc bulging during simple and

complex loads, Heuer *et al.* used a three-dimensional laser scanner device [19]. They observed regions with high compressive strain near the endplates. Furthermore, disc bulging stretched the disc at mid height, causing positive strains in that area both in the axial and in the circumferential direction [19]. However, the above study did not consider the possible effects of different loading rates on the superficial strain distribution.

The review above highlights a lack of understanding about how the load is distributed between the different structures of the spine at different loading rates. In particular, there is a lack of knowledge about the effect of the loading rate on the strain distribution on the surface of the IVD, as a result of the strain rate dependency of the AF and NP. The aim of this work was to investigate the local effects of the loading rate on the strain distribution in the IVD. The hypotheses of this work were:

1. As the IVD stiffens at higher loading rates, the strain distribution the surface around would be different at different loading rates.
2. Pre-conditioning attenuates the strain-rate dependent behaviour of the IVD, thus making differences in strain distribution smaller at the different rates.

2. MATERIALS AND METHODS

2.1 Specimen preparation

Six segments of three vertebrae (L4-L6) were extracted from porcine spines (porcine spines are longer than human ones, up to 6-7 lumbar vertebrae). The animals were sacrificed for alimentary purpose. The specimens were cleaned of all muscles. In order to preserve the natural constraints, the ligaments were left intact, paying attention not to damage the intervertebral discs. The two intervertebral discs were aligned horizontally

in the anterior and lateral plane using a six-degrees-of-freedom clamp. The extremities of the segments were potted in poly-methyl-methacrylate (PMMA) cement.

2.2 Mechanical test

The load was applied using a servo-hydraulic universal testing machine (8032, Instron, high Wycombe, UK). The cranial side of the specimen was fixed to the upper part of the testing machine while the caudal side was placed on a spherical joint which could move on a rail in antero-posterior direction. To generate a compression-flexion, a vertical force with an anterior offset of 25 mm was applied (Fig. 1).

Each test consisted of the application of a three load cycles: one at a fast, one at a medium and one at a slow rate (with a ratio of 1:10:100 between the respective time to reach the full load). In the medium rate the actuator displacement was tuned so that the full load (generating a moment of 5.0 Nm) was reached in 6.7 seconds. In order to allow comparison between the different conditions (fast, medium and slow), the same displacement required to reach the full load at the medium rate was imposed also for the fast and slow load rates (Fig. 2). In the fast rate, the actuator speed was ten times faster than the medium rate, so that the full load was reached in 0.67 s (this was the maximum speed allowed by the frame rate of the DIC system). In the slow rate the full load was reached in 67 s.

Two sets of tests were performed on each specimen: one test (one fast, one medium and one slow cycle, with 60 seconds recovery between load cycles) without conditioning the specimen; one test (same sequence) after conditioning the specimen with 60 cycles at 1 Hz. The specimen between the not-conditioned and conditioned scenarios was left mounted in the testing machine for one hour unloaded in order to allow complete recovery of the height of the two intervertebral discs. In order to verify if the

conditioning was sufficient, a preliminary test of ten cycles was performed with a recovery time of 60 seconds (the same recovery time used in actual tests). A conditioning of 60 cycles was considered sufficient as after such conditioning differences among 10 consecutive cycles were smaller within 1% of the full load.

The load and displacement were acquired using a multichannel data logger (Chassis PXIe-1078, Controller PXIe-8135, DAQ PXIe-6341, National Instruments) at 150 Hz. To keep the specimen hydrated between the first and the second test, the specimens were wrapped in a transparent film in which some water had been sprayed.

2.3 Full-field strain measurement

In order to measure a full-field strain map on the IVD surface, Digital Image Correlation (DIC) was used. The surface of the specimens was dyed with a dark background using a 4% solution of methylene blue (Fig. 1). A white-on-black speckle pattern was prepared on the anterior surface of the specimen with the appropriate dot size, following an optimized procedure [20, 21]. A commercial 3D-DIC system was used (Q400, Dantec Dynamics, Denmark) with its software (Instra 4D, v. 4.3.1, Dantec Dynamics). Two cameras were used (5 MegaPixels, 2440x2050, 8-bit, black-and-white) in order to obtain a stereoscopic vision. Calibration was performed before the tests using a dedicated calibration target (Al4-BMB-9x9, Dantec Dynamics) [22]. The region of interest of the specimens consisted of two intervertebral discs (L4-L5 and L5-L6), and three consecutive vertebrae (L4, L5 and L6), the taken from a lateral view (Fig. 1).

The parameters for the acquisition of the images and for the correlation analysis were preliminarily studied and optimized to minimize errors based on a validated procedure [23]: facet size between 35 and 39 pixels, grid spacing of 21 pixels, contour smoothing of kernel size 5x5 (Table 1). Full-field strain maps of true maximum and minimum

principal strains (ε_1 and ε_2) were computed for all the specimens in correspondence of the two IVDs at the different loading rates and in the not-conditioned and conditioned scenarios.

In order to assess the measurement uncertainties in a known configuration, a pair of images of the unloaded segments were captured for each specimen and analyzed with the optimal hardware and software settings. Being in a zero-strain configuration, any strain different from zero was accounted as measurement error. For the principal strains, a systematic error of less than 100 microstrain and a random error of less than 300 microstrain were found for all specimens.

2.4 Statistical analysis

To investigate the alterations of the strain distribution in correspondence with the two IVDs (L4-L5 and L5-L6 IVDs), two rectangular regions of interest (ROIs) were delimited between the most posterior to the most anterior part of the IVDs (Fig. 3). On these ROIs, the medians over cranio-caudal (longitudinal) lines were computed separately for the two IVDs. The plot of the median values showed the posterior-to-anterior trend of the strain. Then, the median posterior-to-anterior trend was computed between the specimens. As the dimensions of the ROIs depended on the anatomy of each specimen, the data were re-sampled over the same number of points, so as to allow computing the median spatial trend among the specimens.

In order to assess if the differences of the spatial trends of the strains at the three loading rates and in the not-conditioned and conditioned scenarios were statistically significant, a two-sample Kolmogorov-Smirnov test was applied to the strain distributions around the IVDs. All statistical analyses were performed with Matlab (R2019b, MathWorks®, Natick, USA).

3. RESULTS

3.1 Load - displacement

For all the specimens, decreasing the loading rate was associated in a decrease of the peak load (while the same displacement was imposed, Fig. 2), and a decrease of the stiffness. The same trend was found both in the not-conditioned and conditioned scenarios. The variations of peak load can be described assigning a value of 100% to the medium rate (Fig. 4). In the not-conditioned scenario, the load increased by 11% for the fast loading rate, while the load decreased by 29% for the slow rate. Similarly, in the conditioned scenario, the load increased by 14% for the fast loading rate, while the load decreased by 30% for the slow rate.

The difference between the not-conditioned and conditioned scenarios was less than 3% in all the tests.

3.2 Overview of the strain maps

For all specimens in all the tests, the strain maps showed a different order of magnitude of the strain on the surface of the intervertebral discs (ε_1 in the order of +4000/+6000 microstrain, and ε_2 in the order of -25000/-30000 microstrain) as opposed to the vertebrae (ε_1 in the order of +300/+400 microstrain, and ε_2 in the order of -2000/-3000 microstrain) (Fig. 5). In all the cases investigated, flexion of the spine segment induced a bulging of the IVD associated with maximum principal strains (ε_1) in the circumferential direction on the lateral and anterior sides of the two IVDs, while the minimum principal strains (ε_2) were longitudinal. Conversely, the maximum principal strains (ε_1) were in the axial direction (and the associated minimum principal strains ε_2 were circumferential) on the posterior side of the two IVDs, showing an axial stretch in this region.

3.3 Detailed analysis of the effect of the loading rate on the spatial trend

The medians of the trend distribution of strain among the specimens for the two IVDs were computed for the two principal strains (ε_1 and ε_2) for the three loading rates and for the not-conditioned and conditioned scenarios (Fig. 6).

The spatial trend of the principal strains showed an increase in absolute value moving from the posterior to the anterior side of the two IVDs. For the not-conditioned configuration and for all the loading rates, the strain on the posterior side was about 4 times smaller than the strain on the anterior side of L4-L5 and L5-L6 IVD (Fig. 6). For the conditioned configuration, the difference from the posterior to the anterior regions of the two IVDs was slightly higher (the ratio was about 5, Fig. 6). The difference between the spatial trends in the not-conditioned and conditioned scenarios was not statistically significant for both IVDs and for both principal strain components (Two sample Kolmogorov-Smirnov test, $p>0.1$ for all loading rates). This difference between the not-conditioned and conditioned tests was not evident in terms of strain value. Only slight differences appeared in the strain distribution: in the anterior region, near the endplates, with the slow rate, a smoother strain gradient was visible between the most deformed area (IVD) and the least deformed area (vertebra). With the fast rate there was a more abrupt variation between these two areas (Fig. 5).

For the L4-L5 IVD and for L5-L6 IVD, both for not-conditioned and conditioned tests, a slight variation was observed between the fast and slow loading rates for both principal strains (the difference between fast and slow for ε_1 and for ε_2 was less than respectively 1/10 and 1/20 of the maximum measured value, Fig. 6). The difference between the spatial trends due to the loading rate was not statistically significant for both IVDs and for both principal strain components (Two sample Kolmogorov-Smirnov test, $p=0.12$-0.78 in the not-conditioned, and $p=0.22$-0.86 in the conditioned scenario).

4. DISCUSSION

Puzzling findings are reported in the literature concerning the viscoelasticity of the IVD: while the tissues composing the IVD show clear viscoelasticity [11], and FSU show the expected stiffening at high loading rates [17], an increased hysteresis was reported at high loading rates [18]. The aim of this study was to investigate how the strain distribution on the AF changes at different loading rates and if it is affected by conditioning.

A flexion test was performed on 6 porcine segments (L4-L6) applying the load at three different rates (fast, medium and slow) and the full-field strain distribution on lateral surface of the specimens was measured using Digital Image Correlation. To allow direct comparisons, the same displacement was imposed at the different rates, resulting in different values of the peak load in relation to the specimen's viscoelasticity. Furthermore, also the effect of conditioning on the strain distribution was investigated.

During flexion, lower values of maximum and minimum principal strain were reached in the posterior side of the IVDs than in the anterior one, at all loading rates. The gradient of strain from posterior to anterior was gradual without abrupt changes in the absolute value (Fig. 6). This can be explained by NP migrating posteriorly during flexion [4] thus allowing the anterior side of AF to strain more, also in association with the anterior bulging of the disc.

The NP exhibits significant viscoelasticity, depending on the loading rate [6, 7]. At high loading rate, the NP appears stiffer, causing an increase of the internal pressure and of the stiffness, leading to a hardening of the entire structure rate [6, 7]. With a low loading rate, the NP is more fluid, decreasing the stiffness of the structure and absorbing more easily the load [6]. A similar trend is found in the tissues composing the AF [2, 9, 11, 24]. In the present study, the way in which the surface of AF and the endplates were

deformed did not change significantly with different loading rates (Fig. 5). In the transition zones between the disc and the vertebra, only slight differences due to the loading rate appeared, but with no statistical significance: with high loading rates this zone was less uniform showing a more abrupt transition between disc and vertebra respect to what was observed during slow loading rates. Considering that the strain measurement error affecting the present study did not exceed 300 microstrain, effects (if any) must have been smaller than that. A reasonable explanation to our findings is that, as the distribution of strain and the alignment of the principal strain did not change at different loading rates, this means that viscoelasticity affects the entire disc in the same manner. In fact, if different portions of the disc had different viscoelasticity, they would behave stiffer/softer with respect to others at different loading rates, yielding a shift of the strain distribution. Therefore, our findings can be interpreted as an indication of the uniformity of the viscoelastic properties of the different regions of the disc.

During flexion, the directions of the principal tensile strain (ε_1) in the anterior side of the disc were circumferential (and ε_2 was longitudinal, Fig. 5) with the specimen showing a swelling of the disc. Conversely, towards the posterior region of the external part of the disc the two principal strain components were small and similar in magnitude, and therefore the principal directions were more unpredictable. The direction of the strain on the surface of different structures of the spine (vertebrae, endplates, IVDs) remained unchanged at the different loading rates, showing that the way the loads were transferred through the different structures of the column was not affected by the loading rates.

For what concerns the role of conditioning, this did not significantly affect the strain distribution on the surface of AF. Both for the not-conditioned and conditioned scenarios, distribution of strains around the external layers of IVD was similar. The

maximum difference between the not-conditioned and conditioned scenarios was negligible around the surface of the disc and slightly higher (up to 10%) in the anterior side, where more measurement artifacts are also present.

One of the most frequent spine pathologies is disc herniation, consisting in the rupture of the AF and leakage of part of the NP. It is still not completely clear if and to what extent this phenomenon is related to the loading rate [9]. The present findings therefore agree with the results obtained by Gregory *et al.* [25]. They reported that, at strain rates achievable through voluntary motion that could result in herniations of the AF, the tensile response of the AF tissue was not affected by strain rate.

The main limitation of this study relates to the fact that the strain distribution was measured on the external surface of the IVDs. The tools currently available to measure the deformations inside the IVDs (for instance MicroCT, microMRI in conjunction with Digital Volume Correlation, DVC) require long scanning time (minutes-hours) to achieve sufficient image quality. For this reason, they cannot be used to measure the viscoelasticity of the IVD. Conversely, DIC can acquire images with high loading rates: in fact, the rates used in this work spanned from relatively fast movement (0.67 second) to very slow ones (67 seconds) covering the range of daily activities. What was not considered in this analysis is the high loading rate simulating trauma (which can be up to 1/100 of a second).

Another limitation was the use of porcine specimens instead of human specimens. Animal specimens are easier to obtain than human ones. Porcine are similar to human in size and biomechanical response [26, 27]. Conversely, the range of motion (ROM) of porcine spines are different from the ROM of human spines [28]. Therefore, the findings of the present study can be extended to the human spine as a trend, even if possibly not as absolute magnitudes.

5. CONCLUSION

In conclusion this study has shown that the loading rate has negligible effects on the strain on the surface of the annulus fibrosus in the range of loading rates considered here. Similarly, also conditioning did not alter the strain distribution, nor the effect that the loading rate has on the strain distribution. Furthermore, these findings could be useful also for the design of other *in vitro* biomechanical tests and of more realistic numerical models of the spine, knowing what effect different loading rates and conditioning entail on the biomechanics of the intervertebral discs.

Acknowledgments

The Authors wish to thank Dr Marco Palanca for the stimulating discussions about the design of the study, and Dr Federico Morosato for helping during the test sessions.

Conflict of interest statement

There is no potential conflict of interest: none of the Authors received or will receive direct or indirect benefits from third parties for the performance of this study.

References

[1] Gray, H., 1858, "Gray's anatomy," London: Churchill Livingstone.

[2] Ranu, H. S., 1990, "Measurement of pressures in the nucleus and within the annulus of the human spinal disc: due to extreme loading," Proceedings of the Institution of Mechanical Engineers. Part H, Journal of engineering in medicine, 204(3), pp. 141-146.

[3] Thoreson, O., Ekstrom, L., Hansson, H. A., Todd, C., Witwit, W., Sward Aminoff, A., Jonasson, P., and Baranto, A., 2017, "The effect of repetitive flexion and extension fatigue loading on the young porcine lumbar spine, a feasibility study of MRI and histological analyses," Journal of experimental orthopaedics, 4(1), p. 16.

[4] Fennel, A. J., Jones, A. P., and Hukins, D. W. L., 1996, "Migration of the nucleus pulposus within the intervertebral disc during flexion and extension of the spine," Spine, 21, pp. 2753-5757.

[5] Fung, Y. C., 1981, "Biomechanics: Mechanical properties of living tissues," Springer.

[6] Iatridis, J. C., Weidenbaum, M., and Mow, V. C., 1996, "Is the nucleus pulposus a solid or a fluid? Mechanical behaviors of the nucleus pulposus of the human intervertebral disc," Spine, 21, pp. 1174-1184.

[7] Race, A., Broom, N. D., and Robertson, P. A., 2000, "Effect of Loading Rate and Hydration on the Mechanical Properties of the Disc," Spine, 25, p. 662 669.

[8] Chan, S. C., Ferguson, S. J., and Gantenbein-Ritter, B., 2011, "The effects of dynamic loading on the intervertebral disc," European spine journal : official publication of the European Spine Society, the European Spinal Deformity Society, and the European Section of the Cervical Spine Research Society, 20(11), pp. 1796-1812.

[9] Newell, N., Little, J. P., Christou, A., Adams, M. A., Adam, C. J., and Masouros, S. D., 2017, "Biomechanics of the human intervertebral disc: A review of testing techniques and results," Journal of Mechanical Behaviour of Biomedical Materials, 69, pp. 420-434.

[10] Adams, M. A., McMillan, D. W., Green, T. P., and Dolan, P., 1996, "Sustained loading generates stress concentrations in lumbar intervertebral discs," Spine, 21, pp. 434-438.

[11] Kasra, M., Parnianpour, M., Shirazi-Adl, A., Wang, J. L., and Grynpas, M. D., 2004, "Effect of strain rate on tensile properties of sheep disc anulus fibrosus," Technology and Health Care, 12(4), pp. 333-342.

[12] Galante, J. O., 2014, "Tensile Properties of the Human Lumbar Annulus Fibrosus," Acta Orthopaedica Scandinavica, 38(sup100), pp. 1-91.

[13] Ochia, R. S., Tencer, A. F., and Ching, R. P., 2003, "Effect of loading rate on endplate and vertebral body strength in human lumbar vertebrae," Journal of Biomechanics, 36(12), pp. 1875-1881.

[14] Pintar, F. A., Yoganandan, N., and Voo, L., 1998, "Effect of Age and Loading Rate on Human Cervical Spine Injury Threshold," Spine, 23, pp. 1957-1962.

[15] Nuckley, D. J., 2005, "Effect of Loading Rate on the Compressive Mechanics of the Immature Baboon Cervical Spine," Journal of biomechanical engineering, 128(1), p. 18.

[16] Marras, W. S., Knapik, G. G., and Ferguson, S., 2009, "Loading along the lumbar spine as influence by speed, control, load magnitude, and handle height during pushing," Clin Biomech (Bristol, Avon), 24(2), pp. 155-163.

[17] Wilke, H. J., Jungkunz, B., Wenger, K., and Claes, L., 1998, "Spinal segment range of motion as a function of in vitro test conditions: effects of exposure period,

accumulated cycles, angular-deformation rate, and moisture condition," The Anatomical Record, 251, pp. 15-19.

[18] Gay, R. E., Ilharreborde, B., Zhao, K., Boumediene, E., and An, K. N., 2008, "The effect of loading rate and degeneration on neutral region motion in human cadaveric lumbar motion segments," Clin Biomech (Bristol, Avon), 23(1), pp. 1-7.

[19] Heuer, F., Schmidt, H., and Wilke, H. J., 2008, "The relation between intervertebral disc bulging and annular fiber associated strains for simple and complex loading," J Biomech, 41(5), pp. 1086-1094.

[20] Palanca, M., Marco, M., Ruspi, M. L., and Cristofolini, L., 2017, "Full-field strain distribution in multi-vertebra spine segments: an in vitro application of digital image correlation," Med Eng Phys, pp. 1-8.

[21] Lionello, G., Sirieix, C., and Baleani, M., 2014, "An effective procedure to create a speckle pattern on biological soft tissue for digital image correlation measurements," Journal of the mechanical behavior of biomedical materials, 39, pp. 1-8.

[22] Palanca, M., Tozzi, G., and Cristofolini, L., 2015, "The use of digital image correlation in the biomechanical area: a review," International Biomechanics, 3, pp. 1-21.

[23] Palanca, M., Brugo, T. M., and Cristofolini, L., 2015, "Use of digital image correlation to investigate the biomechanics of the vertebra," Journal of Mechanics in Medicine and Biology, 15, pp. 1-10.

[24] Iatridis, J. C., MaClean, J. J., and Ryan, D. A., 2005, "Mechanical damage to the intervertebral disc annulus fibrosus subjected to tensile loading," J Biomech, 38(3), pp. 557-565.

[25] Gregory, D. E., and Callaghan, J. P., 2010, "An examination of the influence of strain rate on subfailure mechanical properties of the annulus fibrosus," Journal of biomechanical engineering, 132(9), p. 091010.

[26] Sheng, S. R., Wang, X. Y., Xu, H. Z., Zhu, G. Q., and Zhou, Y. F., 2010, "Anatomy of large animal spines and its comparison to the human spine: a systematic review," European Spine Journal, 19(1), pp. 46-56.

[27] O'Connell, G., Vreesilovic, E. J., and Elliott, D. M., 2007, "Comparison of Animals Used in Disc Research to Human Lumbar Disc Geometry," Spine, 32, pp. 328-333.

[28] Beckstein, J. C., Sen, S., Schaer, T. P., Vresilovic, E. J., and Elliott, D. M., 2008, "Comparison of animal discs used in disc research to human lumbar disc," Spine, 33, pp. E166 - E173.

[29] Jones, E. M. C., 2018, "A good practices guide for Digital Image Correlation," Internation Digital Image Correlation Society.

TABLES

Table 1. Details of the parameters used for the correlation analysis with the DIC system (reported according to [29])

Parameters for the correlation analysis	
DIC Software Package Name and Manufacturer	Instra 4D, v. 4.3.1, Dantec Dynamics
Distance of the cameras	500 mm
Field of view	about 120 mm by 50 mm
Depth of field	70 mm
Lens aperture	f/22
Frame rate	15 frames per second
Grid spacing	21 pixels
Facet size	between 35 and 39 pixels
Contour smoothing	kernel size 5 x 5

CAPTIONS TO FIGURES

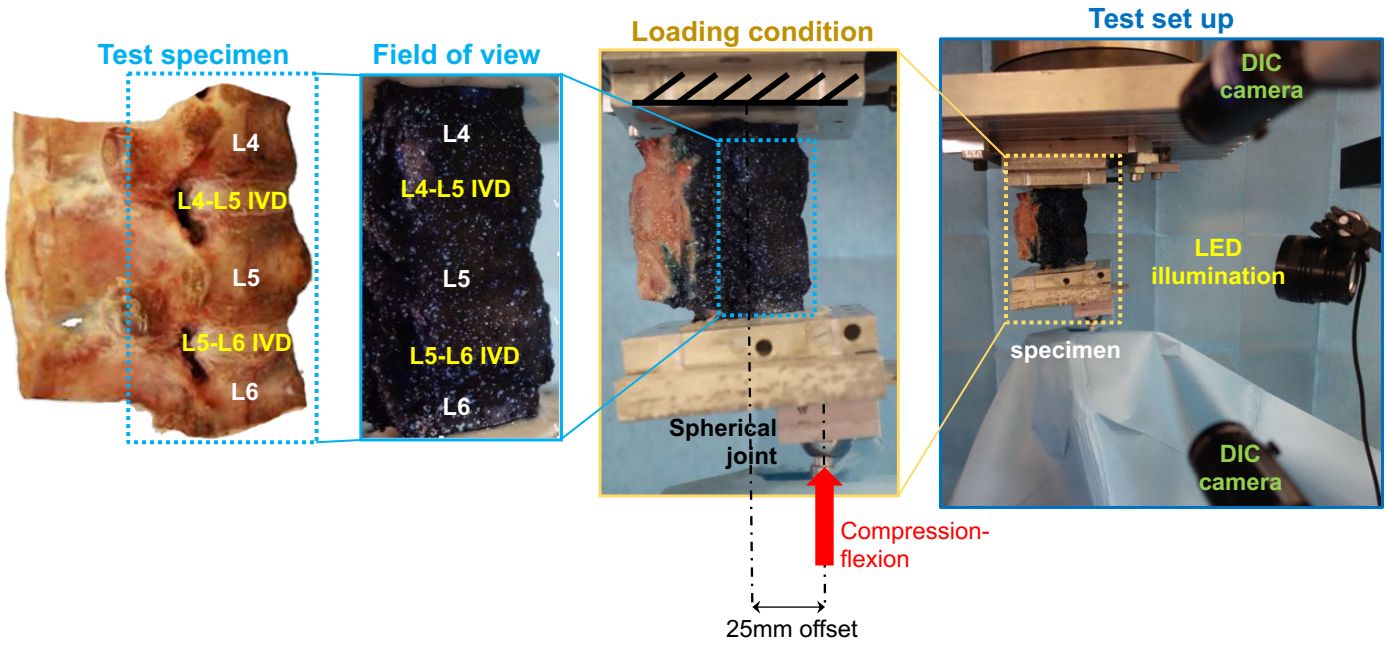

Fig. 1 – Overview of the test configuration and of the DIC system. From left to right: the test specimen (seen from lateral) and the field of view are shown. The vertebrae (L4, L5 and L6) and the intervertebral discs (L4-L5 and L5-L6 IVD) are labelled. The second picture shows the specimen prepared with the white-on-black pattern for the DIC analysis. The last two images show the specimen (lateral view) mounted in the two pots, with the loading system. A compressive force was delivered through a spherical joint, with an offset of 25 mm towards the anterior, simulating in this way a compression-flexion. On the far right, the two cameras of the DIC and the lights are visible.

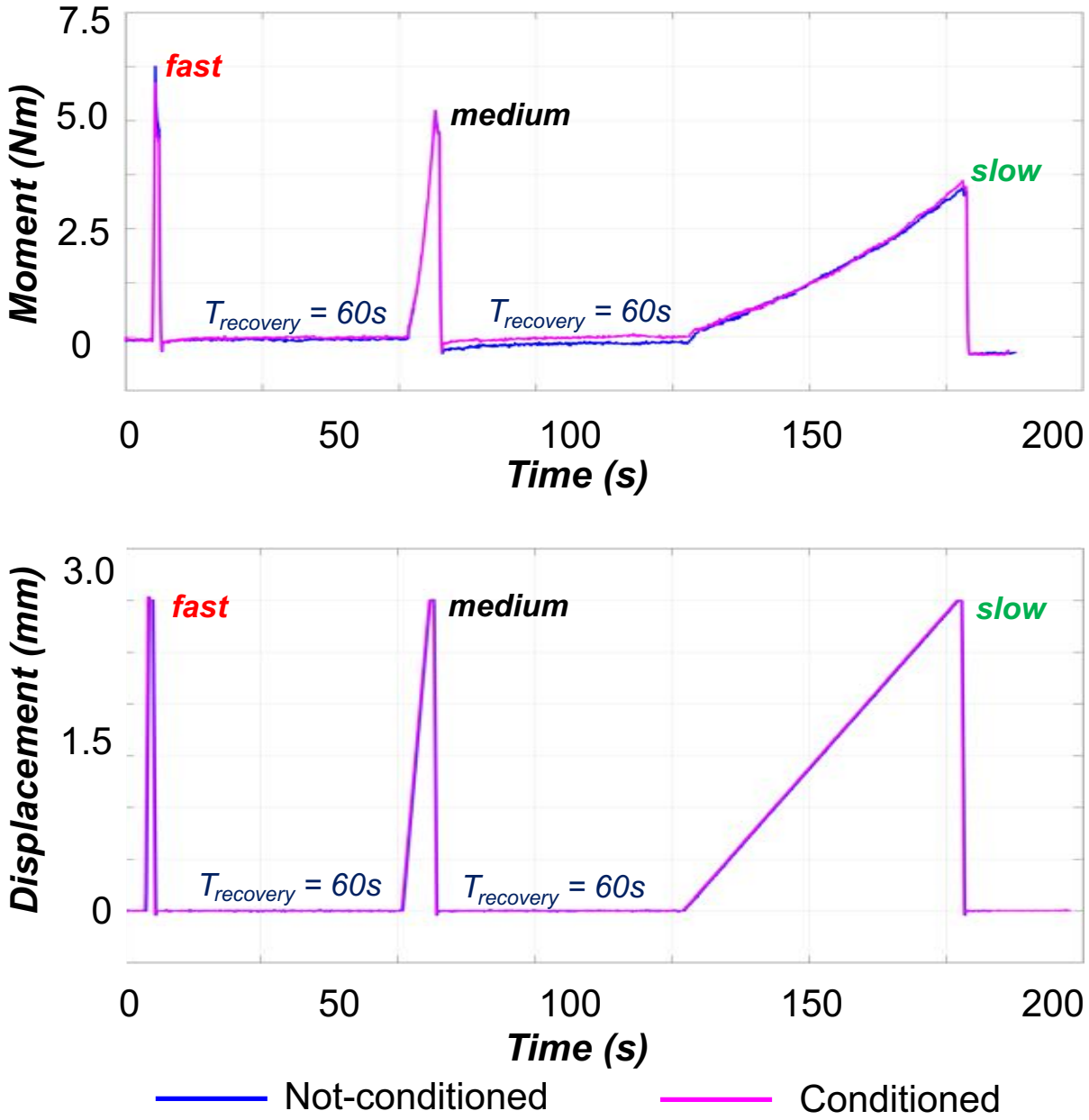

Fig. 2 – Trend of moment and displacement over time for a typical specimen (the trend and the magnitudes were similar for all specimens). The test consisted of fast, medium and slow cycles (with 60 seconds recovery between cycles). The plot on the top shows the load associated with such displacement for the three loading rates and for the not-conditioned and conditioned configurations. The plot on the bottom shows the imposed displacement (the same at all rates, the same in the not-conditioned and conditioned scenarios). As the same displacement was imposed to allow comparison between the loading rates, this resulted in different peak load (the target of 5 Nm was reached at the medium loading rate, whereas the peak load at fast and slow rates were respectively higher and lower than 5 Nm).

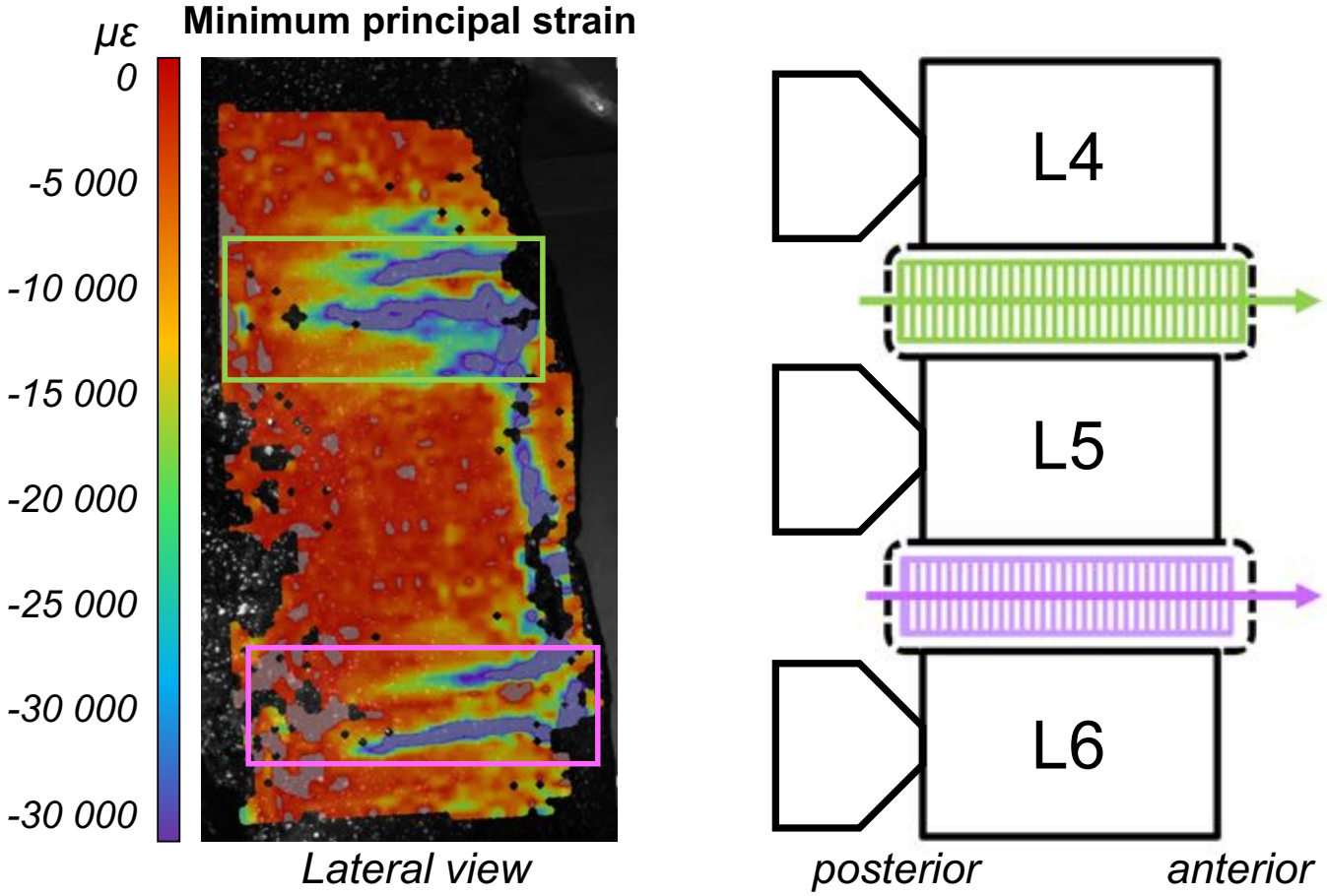

Fig. 3 – On the left, the strain distribution (minimum principal strain) on vertebrae and on the two intervertebral discs is reported from a lateral view for one representative specimen. On the right, a schematic view of the spine is represented. The two rectangles show the ROIs placed on the two IVDs (L4-L5 IVD and L5-L6 IVD) where the spatial trend from the posterior to the anterior side of each ROI was computed as the median values over cranio-caudal (longitudinal) lines.

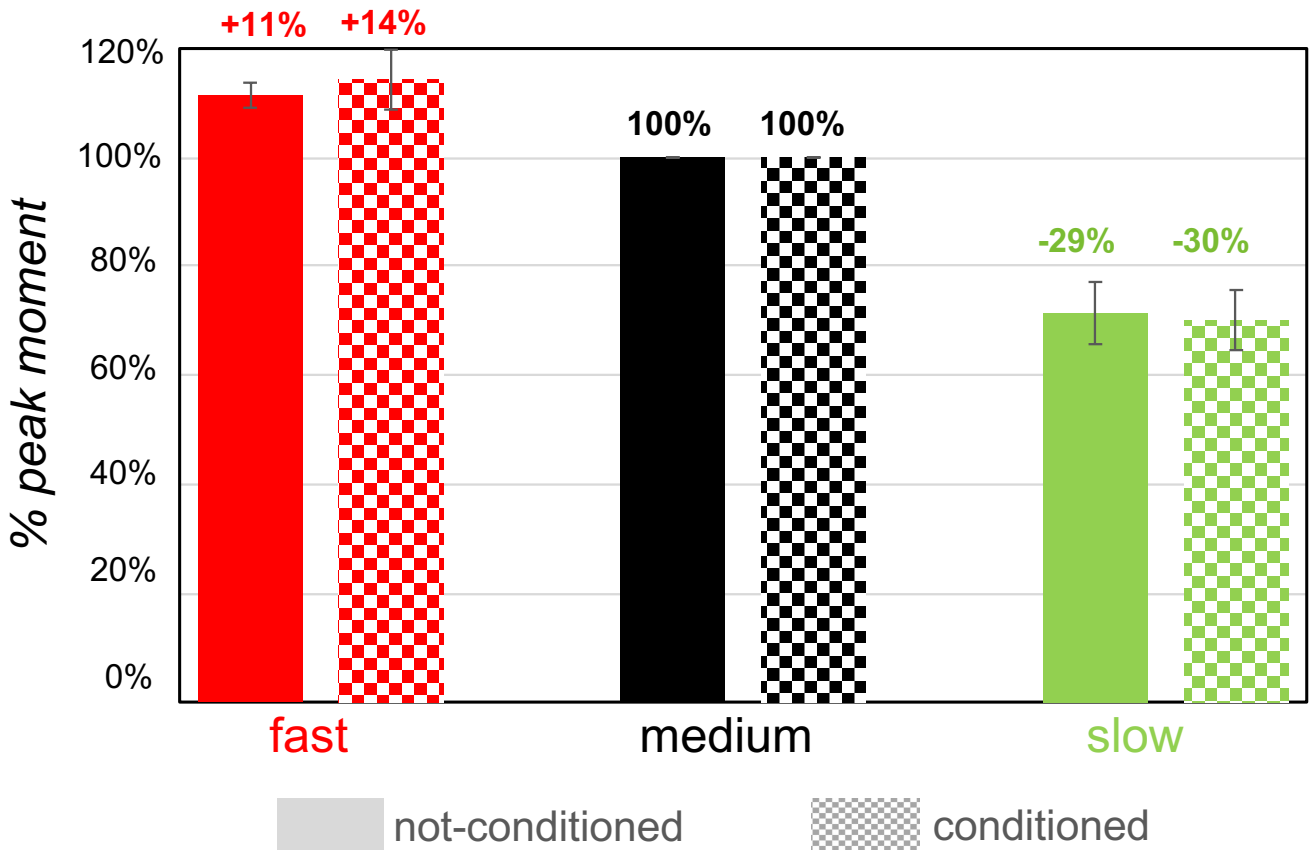

Fig. 4 – In this histogram the differences of peak loads between at the fast and slow loading rate are reported, normalized with respect to the medium loading rate (which corresponds to 100%), both for not-conditioned and conditioned scenarios. The mean and standard deviation over six specimens is reported.

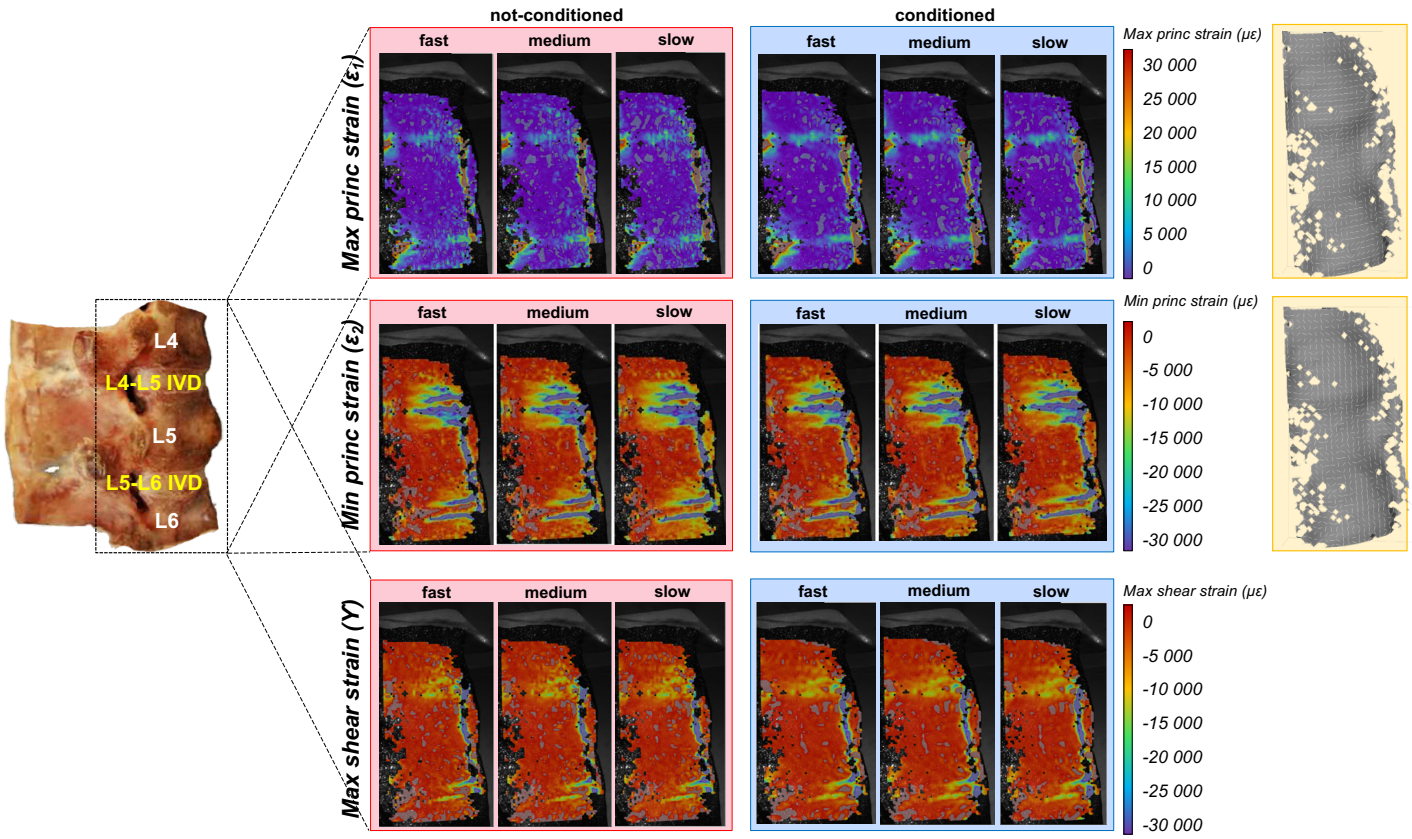

Fig. 5 – The full-field strain distribution on the lateral side of one typical specimen using DIC system is reported. The image on the left shows the test specimen with the three vertebrae and the two intervertebral discs, and the field of view. The images in the center show the maximum and minimum principal strain and the maximum shear strain for the different loading rates (fast, medium, slow) and for both not-conditioned and conditioned scenarios. On the right, the direction for maximum and minimum principal strain are reported.

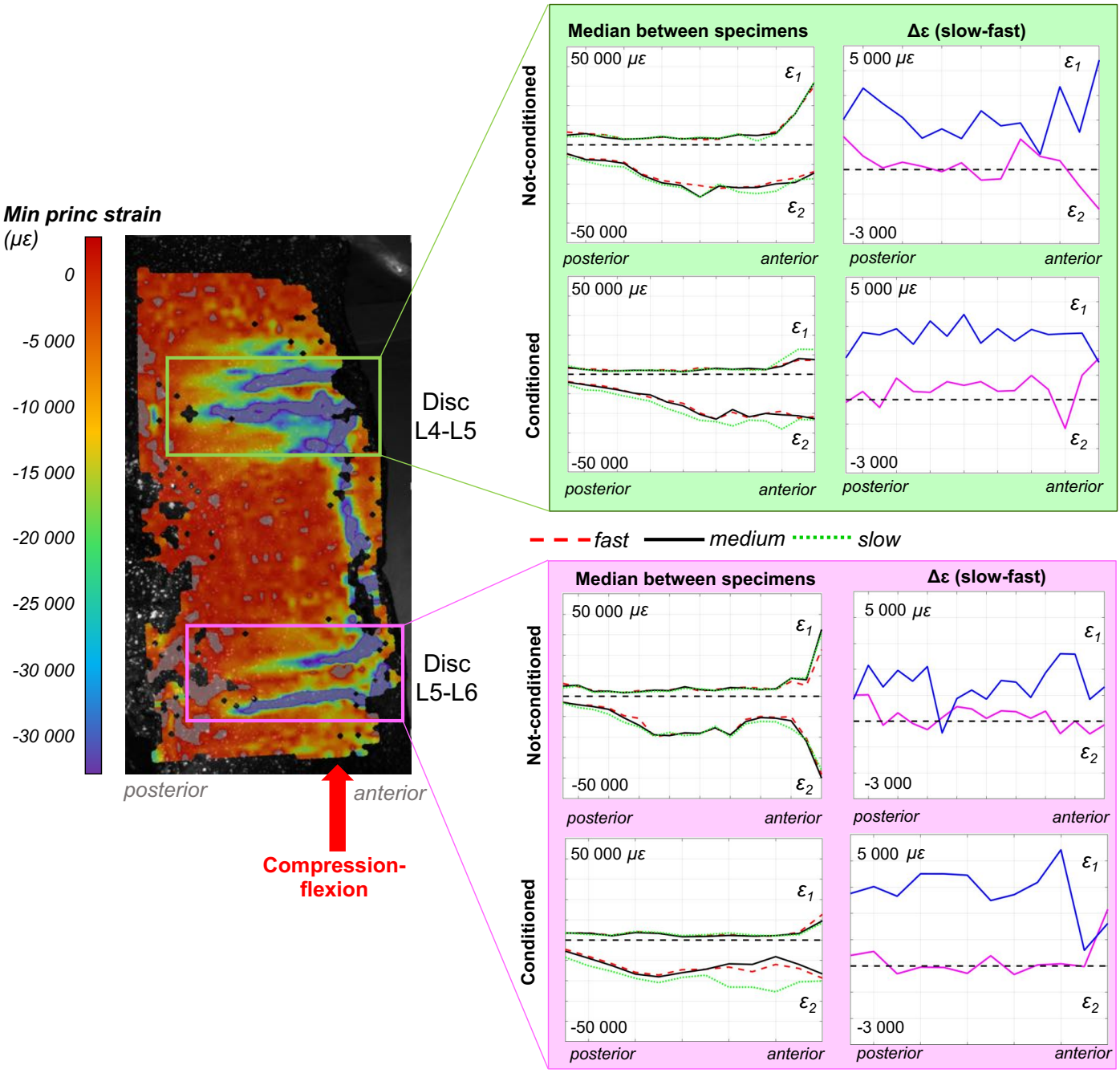

Fig. 6 – On the left, the full-field strain map of minimum principal strain on the lateral side of one typical specimen is shown. The plots on the left side show the spatial trend of the maximum and minimum principal strain (median of the six specimens), respectively for the L4-L5 and L5-L6 IVDs. The plots on the right show the trend of the difference between the slow and fast loading rates of the maximum and minimum principal strains. These trends were reported for the different loading rates (fast, medium, slow) and both for not-conditioned and conditioned scenarios.